Published in final edited form as:
IEEE Trans Image Process. 2012 April ; 21(4): 1823–1833. doi:10.1109/TIP.2011.2170698.

A General Fast Registration Framework by Learning Deformation–Appearance Correlation

Minjeong Kim, **Guorong Wu**, **Pew-Thian Yap**, and **Dinggang Shen**
Department of Radiology and the Biomedical Research Imaging Center, The University of North Carolina at Chapel Hill, Chapel Hill, NC 27599 USA

Dinggang Shen: dgshen@med.unc.edu

Abstract

In this paper, we propose a general framework for performance improvement of the current state-of-the-art registration algorithms in terms of both accuracy and computation time. The key concept involves rapid prediction of a deformation field for registration initialization, which is achieved by a statistical correlation model learned between image appearances and deformation fields. This allows us to immediately bring a template image as close as possible to a subject image that we need to register. The task of the registration algorithm is hence reduced to estimating small deformation between the subject image and the initially warped template image, i.e., the intermediate template (IT). Specifically, to obtain a good subject-specific initial deformation, support vector regression is utilized to determine the correlation between image appearances and their respective deformation fields. When registering a new subject onto the template, an initial deformation field is first predicted based on the subject's image appearance for generating an IT. With the IT, only the residual deformation needs to be estimated, presenting much less challenge to the existing registration algorithms. Our learning-based framework affords two important advantages: 1) by requiring only the estimation of the residual deformation between the IT and the subject image, the computation time can be greatly reduced; 2) by leveraging good deformation initialization, local minima giving suboptimal solution could be avoided. Our framework has been extensively evaluated using medical images from different sources, and the results indicate that, on top of accuracy improvement, significant registration speedup can be achieved, as compared with the case where no prediction of initial deformation is performed.

Index Terms

Deformation prediction; fast image registration; principal component analysis (PCA); support vector regression (SVR)

I. Introduction

Deformable image registration has been extensively investigated in medical image analysis, owing to its importance in removing structural variability that confounds precise detection of anatomical abnormalities. After registration, the anatomical differences among a population of subjects can be quantitatively evaluated according to their deformations with respect to a common template, i.e., using atlas-based morphometry [1]–[3] or inter/intragroup difference comparison [4]–[6].

Deformable registration methods, regardless whether intensity-based [7]–[9] or feature-based [10]–[14], mostly define an objective function that is optimized under various regularization constraints to estimate physically realistic deformations. Possible forms of regularization constraint include elastic energy [15], [16], viscous fluid [17], [18], biomechanical model [19], and Laplacian term [11], [12]. More recent methods have incorporated regularization based on statistical constraints [20]–[24]. However, due to significant template–subject structural shape differences and the high dimensionality of the objective function, determination of accurate template–subject deformations has been a long-standing problem. Accompanying problems include 1) long computation time arising from the need to estimate "large" deformations and 2) vulnerability to ambiguous matching due to structural variability.

A. Motivations

The goal of this paper is to propose a general registration framework to not only reduce the computation time and but also further improve the registration accuracy of the state-of-the-art registration algorithms. To achieve this goal, we present a learning-based registration framework to learn the correlation between image appearances and their respective deformations. For each subject image, we generate an *intermediate template* (IT), which is close in similarity to the subject image, based on a deformation field predicted from the learned correlation model. The need to only estimate the residual deformation field between the IT and the subject image is much less challenging for most of the existing registration methods. This way, a significant amount of computation time can be saved, and the registration accuracy can be improved since the risk of being trapped by local minima will be greatly reduced.

Specifically, our framework consists of three steps in the training stage. First, principal component analysis (PCA) is employed on a set of deformation fields to capture the principal modes of brain deformations using a finite set of parameters. A brain appearance model is then constructed, utilizing low-dimensional image features instead of the whole brain image. After obtaining the statistical models of deformation fields and brain image appearances, we train a deformation–appearance model through support vector regression (SVR), which will help bridge the intrinsic statistics of deformation fields and brain appearances.

When registering a new subject onto the template in the application stage, the initial deformation field and the IT can be rapidly predicted by the trained SVR according to the appearance of the new subject image. Consequently, by requiring only the estimation of the residual deformation from the IT to the subject, the registration time can be greatly decreased. Another obvious advantage is that more reliable registration results can be achieved by our method since the structural difference of a subject from the IT is much smaller than that from the original template. To our knowledge, this paper presents the first attempt to combine, via SVR, statistics of deformation fields and image appearances for not only improving speed but also registration robustness.

To demonstrate the generality of the proposed registration framework, we selected five typical deformable registration algorithms, i.e., hierarchical attribute matching mechanism for elastic registration (HAMMER) [11], [12] (feature-based registration), diffeomorphic demons [25] (intensity-based registration with diffeomorphism constraint), FNIRT [26] (an intensity-based registration algorithm with deformation model parameterized by B-splines), ART [27] (intensity-based registration by nonparametric vector fields, subject to regularity constraints), and SyN [28] (intensity-based registration with a symmetric diffeomorphic optimization) to demonstrate the registration performance before and after integration with our framework. It is worth noting that all these registration methods have been

acknowledged as the state-of-the-art registration methods in [29]. As we will show in the experiment section, we are able to not only speed up their computation time but also improve their registration accuracy.

B. Related Works

Learning-based statistical models have been widely investigated to improve registration accuracy by imposing more realistic registration constraints. However, most works are limited in building learning models based on the deformation fields only. For example, Xue *et al.* [22] construct a statistical model on the wavelet coefficients of deformations to constrain the deformation field during registration. Similar works can be also found in [21] and [23], where the authors build statistical models of B-spline coefficients by principal components analysis. Recently, Glocker *et al.* [20] proposed to hierarchically learn deformation by adaptively treating the control points into two groups, i.e., masters (to encode important information to drive more global deformations) and slaves (to be connected to the masters to estimate more local deformations). In addition, in order to improve the registration accuracy of femur bone computed tomography images, Albrecht *et al.* [24] presented a method for learning deformation statistics from noisy and incomplete data.

There are several other ways, other than the construction of deformation models, to improve registration accuracy. For example, the image similarity metric can be learned in order to increase the accuracy of correspondence matching for shape alignment in [30] and multimodality image registration in [31] and [32]. Wu *et al.* [33] also addressed the importance of determining the appropriate neighborhood sizes for image feature computation. This paper was later extended in [34] to a more general framework based on a boosting algorithm to select the best features and key points. Recently, Yeo *et al.* [35] have proposed an iterative machine learning framework to select the best parameters for an application-specific cost function. They demonstrated that, by improved alignment of cortical foldings, promising results in localizing the underlying cytoarchitecture and functional regions in the cerebral cortex can be obtained.

Ultimately, our learning-based registration framework shares the same motivation as the work of Yeo *et al.*, that is, to boost the performance of the existing registration algorithms. However, we approach this problem from a different perspective in which we attempt to predict an initial deformation field with the help of the correlation information learned between deformation statistics and image appearances. Our goal is to not only improve the registration accuracy but also reduce the computation time, which is of paramount importance to clinical applications.

We have previously developed a method called rapid alignment of brains by building intermediate templates (RABBIT) [36], which is capable of generating the initial deformation fields and the corresponding ITs. The statistical deformation model is first built using a set of training samples by utilizing PCA to characterize the intrinsic warping modes. Then, several ITs are generated by parameterizing the PCA coefficient distribution as a Gaussian distribution and then by performing a uniform coefficient sampling. When registering a new individual subject onto the template, the algorithm automatically determines the most similar precomputed IT as the reference image to which the subject is registered. We note here that the IT is determined based on a simple similarity metric, i.e., the sum of squared difference (SSD), that might not be sufficient for adequately characterizing shapes in a very high-dimensional space. Uniform sampling, as the number of samples exponentially increases, is also inadequate [37]. Our method differs from RABBIT in which: 1) We jointly consider the statistical models of deformation fields and brain appearances and capture their relationship by SVR instead of selecting the IT based on a

simple SSD measurement; 2) several individual subjects might end up with the same IT in RABBIT since they are predetermined by uniform sampling in eigenspace; our method, on the other hand, generates a unique IT for each individual brain adaptively according to its distinctive appearance via the trained SVR; and 3) the number of ITs is fixed in RABBIT, whereas our method can theoretically generate an unlimited number of different ITs.

This paper is structured as follows. In Section II, we describe the proposed registration framework, followed by the details on the statistical models for both deformation and image appearance and also a regression model for correlating deformation and appearance, as well as the prediction of an initial deformation field. We show the experimental results on both real and simulated data in Section III. In Section IV, we conclude this paper.

II. Method

We propose a general framework for improving the registration performance of the existing algorithms by principled estimation of an initial deformation field, which will be discussed in Section II-A. We will explain our learning-based approach in Section II-B, where we apply SVR to learn the correlation between brain appearances and their deformation coefficients. With this learned knowledge, we can automatically determine a good initial deformation field for each individual subject, which we then use to generate a corresponding IT for registration refinement. We will detail each step of the prediction of the IT in Section II-C. Finally, we will summarize our learning-based registration method in Section II-D.

A. Framework for Fast Image Registration

The goal of a deformable registration algorithm is to estimate a dense transformation field $h = \{h(x) | h(x) = x + u_{T\to S}(x), x = (x_1, x_2, x_3) \in \Omega_T\}$ for aligning subject image S to template T, where $u_{T\to S}(x)$ denotes the displacement of a point x in the template image domain Ω_T. On the other hand, inverse transformation field $h^{-1} = \{h^{-1}(x) | h^{-1}(x) = x + u_{S\to T}(x), x = (x_1, x_2, x_3) \in \Omega_S\}$ is used to warp the image in the template space Ω_T to the subject space Ω_S. Most registration algorithms initiate the registration with a null deformation field, i.e., $u_{T\to S}(x) = 0, \forall x \in \Omega_T$. However, for our case, we decompose the overall deformation field $u_{T\to S}$ into two parts: the estimated initial deformation field $u_{T\to IT}$ and the residual deformation field $u_{IT\to S}$, i.e., $u_{T\to S} = u_{T\to IT} + u_{IT\to S}$, as illustrated in the top part of Fig. 1. Here, IT denotes an IT. In our method, $u_{T\to IT}$ is automatically determined according to a regression model learned in the training stage, as shown in the bottom part of Fig. 1. Five steps are involved in this training stage. In *Step 1*, a set of training subject brains $I_0 = \{I_{i,0} | i = 1, \ldots, M\}$ is registered using a registration algorithm, such as HAMMER [11], [12], diffeomorphic demons [25], FNIRT [26], ART [27], or SyN [28] to estimate the deformation field $u_{i,0}$ from the template T to each subject $I_{i,0}$, resulting in a set of deformations $U_0 = \{u_{i,0} | i = 1, \ldots, M\}$ and the corresponding warped images $WI = \{WI_{i,0}(x) = I_{i,0}(h_{i,0}(x)) = I_{i,0}(x + u_{i,0}(x)) | i = 1 \ldots M\}$. Here, $I_{i,0}(h_{i,0}(x))$ denotes warping of an image $I_{i,0}$ using a transformation $h_{i,0}$ (or displacement field $u_{i,0}$). PCA is then employed in *Step 2* to construct a statistical deformation model (called deformation PCA) of U_0, giving us a deformation coefficient vector $\vec{c}_{i,0}$ (as explained in Section II-B1) for each deformation field $u_{i,0}$. Each $\vec{c}_{i,0}$ is a Q-element column vector, where $Q (Q \leq M - 1)$ denotes the number of top-ranked eigenvalues after PCA. The aim of *Step 3* is to solve the *small sample problem*, where we introduce some perturbations to the elements of each deformation coefficient vector $\vec{c}_{i,0}$ to obtain a set of N new simulated deformation coefficient vectors $\{\vec{c}_{i,j}, j = 1, \ldots N\}$. By using both real and simulated deformation coefficient vectors, an enlarged set of (dense) deformation fields $\tilde{U} = \{\tilde{u}_{i,j} | i = 1, \ldots, M, j = 0, \ldots, N\}$ can be obtained. It is worth noting that since $\tilde{u}_{i,j}$ is reconstructed from the perturbed deformation coefficient vector $\vec{c}_{i,j}$, thus $\tilde{u}_{i,0}$ is not equal to $u_{i,0}$. By applying the inverse of each $\tilde{u}_{i,j}$ to each warped image $WI_{i,0}$, a total of $M^2(N + 1)$ simulated training samples,

$\tilde{I}=\{\tilde{I}_{i,k}(x)|i=1,\ldots,M,k=1,\ldots,M\cdot(N+1)\}=\{WI_{i,0}(\tilde{h}^{-1}_{i',j'}(x))|i=1,\ldots,M,i'=1,\ldots,M,j'=0,1,\ldots,N\}$, can be obtained, where $WI_{i,0}(\tilde{h}^{-1}_{i',j'}(x))$ denotes transforming an image $WI_{i',0}$ to the subject image space by using the inverse transformation field $\tilde{h}^{-1}_{i,j}$. Although our framework does not explicitly impose diffeomorphism on the deformation field, in practice, deformations can be reasonably inverted using the method proposed in [38].

Steps 4 and 5 involve constructing the brain appearance model based on the data set $\tilde{I}$. To build an efficient regression function with better generalization performance, we propose employing signature images $SI=\{SI_{i,k}|i=1,\ldots,M,k=1,\ldots,M\cdot(N+1)\}$ that capture brain outlines and also the boundaries along the interfaces of white matter (WM), gray matter (GM), cerebrospinal fluid (CSF), and ventricular (VN) CSF of $\tilde{I}_{i,k}$ instead of directly using all voxels in $\tilde{I}_{i,k}$. After calculating the eigenvalues and eigenvectors of SI by PCA (called signature PCA), we select D eigenvectors with the largest eigenvalues to project SI to obtain their low-dimensional representations called signature vectors $SM_{D\times M^2(N+1)}$, where each column of SM is the signature vector of the corresponding $SI_{i,k}$. We will give a more detailed description of this in the next section.

The key of our approach is the use of a support regression machine to bridge the statistical deformation model with the brain appearance model, as shown in the middle part of Fig. 1. We train Q support vector machines independently, and each of them will make its own regression between each deformation coefficient and the whole set of signature vectors SM. Therefore, when registering a new subject S onto the template T, its signature vector is first calculated according to its signature image. Then, through a set of Q trained support vector machines, we can predict a unique deformation coefficient vector $\vec{c}_S$ for the subject S, which can be, in turn, used to construct an IT and an initial deformation field $u_{T\rightarrow IT}$. We note here that the shape difference between IT and S is quite small, as illustrated by the right two brain images at the top part of Fig. 1. Finally, many existing registration algorithms can be employed to estimate the rest of the deformation $u_{IT\rightarrow S}$. The IT allows this to be done more efficiently by avoiding the direct subject-to-template registration.

B. SVR on Statistical Deformation and Image Appearance Models

Here, we will describe our learning-based framework (outlined at the bottom part of Fig. 1). We will describe how a PCA-based method is used to build the statistical models of both deformation fields (see Section II-B1) and image appearances (see Section II-B2), followed by how we train a set of SVR models to establish deformation–appearance correlation (see Section II-B3).

1) Statistical Model of Deformation Fields—Given a set of M brain images I_0, their respective deformation fields U_0 can be estimated by many existing registration algorithms such as HAMMER [11], [12], diffeomorphic demons [25], FNIRT [26], ART [27], or SyN [28]. After arranging each deformation field into a vector representation, we apply PCA on these M vectors and obtain a statistical deformation model that captures the statistical variations of these deformation fields U_0. Specifically, the eigenvectors of covariance matrix of the deformation fields represent the principal modes of variation, and their eigenvalues indicate the magnitude of deformation variation in the direction of the corresponding eigenvector. Usually, only a small number of eigenvectors with the largest eigenvalues will be used to approximate the original data since they characterize the principal shape changes. For instance, by selecting $Q=25$ eigenvectors after employing PCA on 50 deformation fields, we are able to represent almost 95% of the total energy of shape variations. The reconstructed deformation field $\hat{u}_{i,0}$ of each $u_{i,0}\in U_0$ with the Q largest eigenvectors can be formulated as

$$\hat{\boldsymbol{u}}_{i,0} \approx \bar{\boldsymbol{u}} + \sum_{q=1}^{Q} c_{i,0}^{q} \sqrt{\lambda_u^q} \Phi_u^q \tag{1}$$

where $\bar{u}$ denotes the mean deformation field, and λ_u^q and Φ_u^q are the eigenvalues and eigenvectors of covariance matrix of deformation samples, respectively. Each deformation field $u_{i,0}$ is now represented by $\hat{u}_{i,0}$ in a subspace (spanned by the Q largest eigenvectors) with a deformation coefficient vector $\vec{c}_{i,0}=[c_{i,0}^1,\ldots,c_{i,0}^q,\ldots,c_{i,0}^Q]^T$, where $c_{i,0}^q=(\Phi_u^q)^T(u_{i,0}-\bar{u})/\sqrt{\lambda_u^q}$. Note that $\vec{c}_{i,0}$ is a Q-element column vector.

2) Statistical Model of Image Appearances

Generating More Training Samples: We are often faced with the problem of having a limited number of training samples in I_0. To remedy this, we simulate additional brain images based on the generated statistical model of U_0 with the hope of increasing the robustness of estimation of the brain appearance model. Unlike the simulation method used in RABBIT [36], which parameterizes the distribution of $\vec{c}_{i,0}$ as a Gaussian model and simulates new deformations by uniform sampling in a PCA-represented subspace (see [37, Fig. 1]), we generate MN new deformation coefficient vectors $\vec{c}_{i,j}=\vec{c}_{i,0}+\vec{p}_{i,j}$ ($i=1,\ldots,M$, $j=1,\ldots,N$) by perturbing $\vec{c}_{i,0}$ with $\vec{p}_{i,j}$. Specifically, $\vec{p}_{i,j}$ is generated by randomly sampling around the location of vector $\vec{c}_{i,0}$ in the Q-dimensional subspace. It is worth noting that $\vec{p}_{i,0}=\mathbf{0}$ since $\vec{c}_{i,0}$ is the baseline of all $\vec{c}_{i,j}$ ($1\le j\le N$). Therefore, the simulated deformation fields can be constructed using

$$\tilde{u}_{i,j} \approx \bar{u} + \sum_{q=1}^{Q} \left(c_{i,0}^q + p_{i,j}^q\right) \sqrt{\lambda_u^q} \Phi_u^q. \tag{2}$$

Fig. 2 gives an illustration of the procedure we use in simulating brain samples. We assume that we have $M=5$ subjects, each with $N=4$ perturbations. After registration using HAMMER, diffeomorphic demons, FNIRT, ART, or SyN, these subjects are aligned onto the template (black circle) and are denoted as $WI_{i,0}$ ($i=1,\ldots,M$). In order to cover as much of the brain space as possible, we continue to generate N new simulated deformation fields $\tilde{u}_{i,j}$ ($j>0$) for each $\tilde{u}_{i,0}$, according to (2). There are, hence, $M\cdot(N+1)$ deformations in total. As shown in Fig. 2, we consider all the brains as nonuniformly distributed in the high-dimensional manifold. In order to cover as much as possible different image appearances, we apply all $M\cdot(N+1)$ deformations to each real training sample, obtaining $M^2\cdot(N+1)$ simulated images in total. In Fig. 2, each blue circle denotes a set of M simulated images of subject j ($j=0,1,\ldots,N$).

Statistical Model of Image Appearances: Similar to the method presented in the previous section, the brain appearance model can be constructed based on an enlarged set of brain images $\tilde{I}$ [39]. However, in order to obtain a brain appearance model feasible for estimating the regression model described in the next section, we employ a number of strategies to reduce the dimensionality of $\tilde{I}$ before building the brain appearance model.

For each brain image $\tilde{I}_{i,k}$ ($i=1,\ldots,M$, $k=1,\ldots,M(N+1)$) $\in\tilde{I}$, the uninformative background voxels will be first cropped away by computing a bounding box that covers the whole brain volume. The image will be then downsampled by a factor of 4 in each dimension, obtaining $\tilde{I}'_{i,k}$, as shown in the second column of Fig. 3. To represent the shape

variations of each brain image $\tilde{I}'_{i,k}$, we segment the images into four tissue types, i.e., WM, GM, CSF, and VN, and extract the brain outlines and boundaries along the interfaces between them as shape descriptors for constructing the signature image $SI_{i,k}$ (see the third column of Fig. 3). Tissue classification consisted of two steps. First, we used the fast algorithm (FSL, http://www.fmrib.ox.ac.uk/fsl/) to segment the whole brain into WM, GM, and CSF. Second, we warp the ventricle label of the template to the subject space to label the subject ventricle. It is worth noting that our purpose of employing tissue classification here is not for accurate segmentation but for extracting boundary information. Therefore, other kinds of edge features can be also used here, e.g., Canny edge filter or even simple intensity gradient map. Next, we apply PCA (called as signature PCA) to whole signature images. Afterward, the signature PCA model is applied to each signature image $SI_{i,k}$ to obtain a low-dimensional representation by a signature column vector $\vec{sm}_{i,k}$

$$\vec{sm}_{i,k} = \left[sm^1_{i,k} \ldots sm^d_{i,k} \ldots sm^D_{i,k} \right]^T, \quad sm^d_{i,k} = \frac{(\Phi^d_{sm})^T (SI_{i,k} - \overline{SI})}{\sqrt{\lambda^d_{sm}}} \tag{3}$$

where $\overline{SI}$ denotes the mean shape of all signature images, and λ^d_{sm} and Φ^d_{sm} are eigenvalues and eigenvectors of their covariance matrix, respectively. Only the top D ranked eigenvectors, representing around 70% the sum of all $M^2(N+1)$ eigenvalues, are selected (see the fourth column of Fig. 3) so that the appearance model is less sensitive to the less important shape deviations. By arranging all column vectors $\vec{sm}_{i,k}$ into a matrix, we obtain $SM_{D \times (M^2(N+1))} = [\vec{sm}_{1,0}\ \vec{sm}_{1,1}, \ldots, \vec{sm}_{M,M+MN}]$ (see the rightmost part of Fig. 3). In the following section, we will describe how we train the SVR models to estimate the correlation between deformation coefficient vectors $C_{Q \times (M^2(N+1))} = [\vec{c}_{1,0}\ \vec{c}_{1,1}, \ldots, \vec{c}_{M,M+MN}]$ and signature matrix SM.

3) Regression on Deformation–Brain Appearance Model—An important part of our learning-based registration approach is the utilization of SVR models to learn the correlation between brain appearances and their corresponding deformation coefficients, and then use them to predict a set of deformation coefficients when given a new brain image for registration (as illustrated in Fig. 4). Specifically, we will train Q SVR models, each of them determining a nonlinear regression function $f_q (q = 1 \ldots Q)$ between signature matrix SM (see Section II-B2) and each deformation coefficient from a respective row of matrix C (see Section II-B2).

Note that SVR [40], [41] is a supervised learning technique for finding nonlinear mapping functions that correlate a number of input variables (features) with the values of a continuous output variable (target). Here, the features are the signature matrix $SM_{D \times (M^2(N+1))}$, and the targets are the rows of the deformation coefficient matrix $C_{Q \times (M^2(N+1))}$ [see (3)]

$$\left\{ f_q \left(SM, \vec{e}^T_q \cdot C \right) | q = 1 \ldots Q \right\} \tag{4}$$

where f_q denotes the qth SVR model in Fig. 4. $\vec{e}^T_q$ is the transpose of a Q-dimensional column vector with all zeros except the qth element, which has a value of 1. An identical set of signature vectors SM is used as the features of all regression models, and the qth row of deformation coefficient matrix C is independently used as the target for the qth regression model f_q.

We select the Gaussian radial basis function as the kernel function due to its good performance in classification and regression [42]. In our method, we estimate the kernel size based on the distribution of each signature vector $\overrightarrow{sm}_{i,k}$ by computing the average of the distances from all possible pairs of $\overrightarrow{sm}_{i,k}$. A recently proposed algorithm [41], which uses an intensive loss function ε to achieve the global minimum with reliable generalization bound, has been used to determine f for all SVR models. Parameter ε is used to control the width of the insensitive zone that penalizes the training data outside this zone. Constant $\gamma > 0$ determines the tradeoff between the flatness of f and the tolerance to deviation larger than ε. The values of ε and γ can be calculated as [43]

$$\varepsilon=\tau \cdot \sigma_s \sqrt{\ln (M^2(N+1))/(M^2(N+1))} \quad (5)$$

$$\gamma=\max (|\bar{c}+3\sigma_c|, |\bar{c} - 3\sigma_c|) \quad (6)$$

where σ_s is the standard deviation of distances between all pairs of $\overrightarrow{sm}_{i,k}$, τ is an empirical constant, and $M^2(N+1)$ is the number of signature vectors used as the features for regression. $\bar{c}$ and σ_c are the mean and the standard deviation of overall deformation coefficients $\vec{c}_{i,k}$, respectively.

C. Predicting the IT and Initial Deformation Field

After training the regression models, the ITs can be predicted to facilitate the registration by achieving robust results in a significantly reduced time. For a new subject S, its signature vector $\overrightarrow{sm}_s$ will be first computed by projection onto the top D eigenvectors (see Section II-B2) after the affine alignment to the template by FSL FLIRT [44]. Deformation coefficients $\vec{c}_s=(c_s^1, c_s^2, \ldots, c_s^Q)$ can be then predicted one by one through each trained SVR model (see the bottom part of Fig. 4). Next, it is straightforward to obtain the initial deformation $u_{T\to IT}$ for the subject by (1). The IT for S can be then generated by warping the template with respect to $u_{IT\to T}$. Fig. 1 illustrates the whole procedure of registering template T to subject S with the proposed registration method. Unlike traditional registration algorithms, we simply need to estimate only the remaining deformation field from the IT to the subject, and this helps save a significant amount of computation cost and circumvent the error-prone approach of estimating large deformations from the original template to the subject. Upon estimating $u_{IT\to S}$ (by the existing registration method), deformations $u_{T\to IT}$ and $u_{IT\to S}$ can be concatenated. Fig. 5 shows images from each step of the proposed method for template (a) and subject image (b). First, an IT (c) is estimated. The IT is then registered to the subject image. By concatenating the deformations from the template to the IT and from the IT to the subject, we can warp the template to the subject, as shown in (d), which gives a result comparable to HAMMER (e).

D. Summary of our Fast Registration Framework

Our registration method is capable of achieving robust registration results with much less computation time by predicting a good initial deformation field and an IT for a subject image under registration. The whole registration framework can be summarized in two stages, i.e., training and application stages. They are summarized below.

Training Stage

t1) Collect M deformation fields u_i, $i = 1, \ldots, M$, each estimated by deformable registration (using HAMMER, diffeomorphic demons, FNIRT, ART, or SyN) between a template T and M brain images $\{I_{i,0}, i = 1, \ldots, M\}$.

t2) Perform PCA on the deformation fields to construct a statistical deformation model with eigenvectors Φ_u^q, eigenvalues $\sqrt{\lambda_u^q}$, and mean deformation field $\bar{u}$.

t3) For each $\vec{c}_{i,0}$ (calculated from each deformation field sample with PCA), introduce N perturbations to simulate a set of new deformation coefficient vectors $\vec{c}_{i,j}$ ($j = 1, \ldots, N$). Then, reconstruct dense deformation fields $\tilde{u}_{i,j}$ ($i = 1, \ldots, M, j = 0, \ldots, N$) by (2). Next, invert $\tilde{u}_{i,j}$ and apply $\tilde{u}_{i,j}^{-1}$ onto each $WI_{i,0}$ to obtain $M^2(N+1)$ simulated brain images $\tilde{I}=\{\tilde{I}_{i,k}(x), i=1,\ldots,M, k=1,\ldots,M\cdot(N+1)\}=\{WI_{i,0}(h_{i',j'}^{-1}(x))|i=1,\ldots,M, i'=1,\ldots,M, j'=0,1,\ldots,N\}$.

t4) Construct the signature image for each simulated brain image $\tilde{I}_{i,k}$ (see Section II-B2).

t5) Create signature matrix $SM_{D\times(M^2(N+1))}$. Each column of matrix SM is a low-order representation of a signature image obtained by projection onto the top D eigenvectors by (3).

t6) Train Q regression models $(SM, \vec{e}_q^{\,T}\cdot C)$ through SVR by regarding signature matrix $SM_{D\times(M^2(N+1))}$ as inputs and each row of deformation coefficient matrix $C_{Q\times(M^2(N+1))}$ as target values.

Application Stage

a1) Calculate the signature vector $\vec{sm}_s$ for a new subject s.

a2) Predict the deformation coefficient $\vec{c}_s=(c_s^1, c_s^2, \ldots, c_s^Q)$ through the Q learned SVR models.

a3) Generate an initial dense deformation field $u_{T\to IT}$ according to $\vec{c}_s$ by (1) and warp template image T using $u_{IT\to T}$ to obtain an IT.

a4) Use a deformable registration method (e.g., HAMMER, diffeomorphic demons, FNIRT, ART, or SyN) to estimate the remaining deformation field $u_{IT\to S}$ from the IT to the subject S and then concatenate $u_{T\to IT}$ and $u_{IT\to S}$ for obtaining the final deformation field.

III. Experimental Results

The accuracy, robustness, and speed of the proposed learning-based registration method are comprehensively evaluated in comparison with several typical deformable registration algorithms. We first validate the advantages of our registration framework by regarding the simulated deformations as the ground truth. Here, we take HAMMER as an example and demonstrate the superiority of the proposed framework over RABBIT [36]. Additional experimental results are reported on real elderly brains and the public data sets (nonrigid image registration evaluation project (NIREP) [45] and Laboratory of Neuro Imaging (LONI) [46] data set). Our registration framework can be easily integrated with a number of the existing registration algorithms for immediate improvement of registration performance. To show this, we use HAMMER (feature-based registration method), diffeomorphic demons [25] (intensity-based registration method with diffeomorphism constraint), FNIRT [26] (intensity-based registration method with deformation field parameterized with the B-splines), ART [27] (intensity-based registration by nonparametric vector fields, subject to regularity constraints), and SyN [28] (intensity-based registration with symmetric diffeomorphic optimization) as the example registration methods in the subsequent

experiments. Note that these methods have been acknowledged as state of the art in a recent survey paper [29].

A. Experiments on Simulated Data

In the following experiment, we use the HAMMER registration algorithm as the baseline and compare the registration performance with RABBIT and our proposed method. It is worth noting that both RABBIT and our method use HAMMER to complete the estimation of the rest of the deformation field after predicting the initial deformation field.

Brain Images With Simulated Deformations—We simulated a set of deformation fields using the algorithm proposed in [47] to serve as ground truth for evaluation. The baseline images are selected from the Baltimore Longitudinal Study of Aging (BLSA) [48] data set. Specifically, we simulated three groups of deformation fields (10 in each group) with different mean magnitudes of deformations, i.e., 2 mm (Group 1), 4 mm (Group 2), and 6 mm (Group 3). Fig. 6 shows, for each group, some typical images generated by warping the template with the simulated deformation fields. We then estimated the deformation field between the simulated subject and the template by HAMMER, RABBIT, and our method, respectively. By comparing the residual error (average of the voxel-wise Euclidean distances) between the estimated deformation fields with respect to the ground truth, we can quantitatively measure the registration accuracy. From the average residual errors shown in Table I, it is clear that our method outperforms original HAMMER and RABBIT, particularly for the simulated subjects with larger deformations, thus showing the robustness of our registration framework.

B. Experiments on Real Data

Real Elderly Brain Images—We used $M = 50$ elderly magnetic resonance (MR) images randomly selected from the BLSA [48] data set for training and another 50 images for validation. Each image has a size of 256 × 256 × 124 and a resolution of 0.9375 mm × 0.9375 mm × 1.5 mm. The images were segmented into four tissue types, i.e., WM, GM, CSF, and VN, respectively. Before training, affine registration [44] was performed on all training samples to remove global translation, rotation, and scaling. We then estimated the deformation fields of all these images with respect to a template by using HAMMER. Applying PCA, we built a statistical deformation model with 49 modes from the 49 eigenvectors with nonzero eigenvalues, and each deformation field was represented by 25 PCA coefficients for covering 95% of the variability. For denser sampling of the deformation field space, we applied $N = 4$ perturbations, thus giving us a total of $M(N + 1) = 50 \times 5 = 250$ deformation samples and $M^2(N + 1) = 12\,500$ simulated brain images by inverse deforming the 50 normalized images in the template space. We used half (i.e., 6250) of the deformation–image pairs (corresponding to 25 original MR brain images) for training and the other half for validation. We note here that a sufficient number of samples are important for training a robust statistical model. The samples used for training and validation can be considered independent since there is no overlap between the original MR images used for training and testing.

The results show that the average prediction error based on predicted deformation coefficients is 1.5% on the training data and 5.7% on the validation data. The prediction error was computed based on the ratio of the difference between the predefined deformation coefficients and their estimated ones. These results indicate that our model is able to predict very good initial deformations for the validation data, which can significantly help reduce computation cost and increase registration robustness, as reported in Section III-B. Since the validation data were not used for training, the error in estimating its deformation coefficients is larger than the training error, which is reasonable. To demonstrate the importance of using

perturbation for generating sufficient samples, we further evaluated the performance of our statistical model without perturbation, and the average prediction error on the same validation data increases to 15.9%, which is more than two times higher than that using the deformation perturbation strategy.

Given a new image, we first align it linearly to the template space, and then construct its signature vector by downsampling, feature extraction, and dimensionality reduction, which we can finally use to predict the initial deformation. To evaluate the quality of the predicted deformation, we use other 50 images that have not been included in the training. Some test images are shown in Fig. 7(b), and it can be observed that they are structurally very different from the original template shown in Fig. 7(a). Fig. 7(c) and (d) shows the intermediate registration results given by HAMMER in low (downsampled with a factor of 4) and middle resolution (downsampled with a factor of 2), respectively. Fig. 7(e) and (f) shows the ITs generated by RABBIT and our learning-based method, respectively. To help visual comparison, we delineate the brain outline of each subject image (as shown by the green lines) and superimpose it on the intermediate results/templates. It can be observed that the ITs generated by the two learning-based methods are much better than those intermediate registration results obtained by HAMMER in low and middle resolution. Closer inspection further shows that the ITs given by our learning-based method outperform those of RABBIT, particularly in the regions pointed by the red arrows.

For quantitative evaluation of those estimated ITs/results, we calculate the Dice ratios [49] for those 50 test images to gauge the overlap of GM, WM, and VN after initial registration. The results, as shown in Table II, indicate that the intermediate results given by HAMMER in low resolution yield the lowest Dice ratios. The next lowest value is given by HAMMER performed up to the middle resolution. Compared with RABBIT, our learning-based method accomplishes the higher Dice ratios for all tissue types. All these experimental results indicate the advantage of our method over HAMMER and RABBIT in predicting better ITs. Note that, here, HAMMER used low resolution, or along with midresolution, to estimate the intermediate deformation or template.)

LONI LPBA40 Data—Our framework is general enough to allow incorporation of different registration algorithms. To demonstrate this, we utilized HAMMER, diffeomorphic demons, FNIRT, ART, and SyN algorithms1 for obtaining the deformation fields from the training samples, constructing the statistical deformation model, and estimating the residual deformation from the IT to the subject. Note that our intention here is not to compare the performance between HAMMER, diffeomorphic demons, FNIRT, ART and SyN, but to demonstrate the improvement that our framework can yield.

The LONI LPBA40 data set is used for this experiment. This data set consists of 40 subjects, each manually labeled with 54 regions of interest (ROIs). For the five registration methods under evaluation, we incorporated them into our learning-based registration framework. For each case, we randomly chose one subject as the template. For the remaining 39 subjects, we used 20 subjects for training and 19 subjects for testing. The Dice ratios, for all ROIs of the 19 subjects yielded by HAMMER, diffeomorphic demons, FNIRT, ART, and SyN, are compared for cases with and without our framework. The averaged Dice ratios over 54 ROIs by three registration algorithms before and after integration with our registration framework

[1]Since the software of ART and SyN do not provide the interface for the initialized deformation field, the integrated version of these two methods considers IT images (generated by our learning-based method in Section II-C) as the target images in their standard registration procedure. That is, for each new subject, we first linearly register it to the template, and then use our method to estimate an IT for it. Then, we use ART (or SyN) to register the subject onto the IT. Thus, with the known deformation from the template to the IT, we can bring the warped subject in the IT space to the real template space. This way, all subjects can be finally warped onto the same real template space for checking their overlap on the corresponding ROIs.

are listed in Table III. The improvement for all cases is statistically significant ($p < 0.05$, two-sample t-test). In Fig. 8, we show the Dice ratio for each ROI, with blue for the original five registration methods on average and pink for the five methods after integrating with our registration framework. Our framework yields a noticeable increase in overlap ratios for most of ROIs.

C. Generalization

In all previous experiments, we all used a subgroup of the same data set for training and performed testing based on the remaining data. However, anatomical structures might differ from one group to another. For example, the images of elderly brains differ from those of younger brains because of aging. Here, we further evaluate the generalization performance of our proposed learning-based framework by training the correlation model using one data set and applying to it to another data set. Specifically, we used 40 images from the LONI LPBA data set for training and 16 images from the NIREP (with 32 manually labeled ROIs) for testing. We randomly chose one subject from the LONI data set as the template and employed HAMMER to generate the deformation fields for training. The images from NIREP are used for testing the registration performance. After registration, we computed the mean overlap ratio of ROIs between the template and each of the 16 aligned NIREP images. The averaged overlap ratio of each ROI of the 16 aligned images is shown in Fig. 9. The overall Dice ratios in all 32 ROIs are 66.8% by the original HAMMER, and they are 67.4% after integration with our framework, indicating that the two methods have comparable accuracy while taking less computation time (see Section III-D).

A similar experiment has been conducted using RABBIT reported in [36], which achieves about 68% overlap ratio for NIREP data. However, the difference between their experiment and ours is that, in their experiment, all training images (Open Access Series of Imaging Studies database [50]) are aligned to a template selected from the test data set (NIREP database). For comparison, we also performed the same experiment using our method and achieved 69.1%, which is better than RABBIT's result. Moreover, the computation time is also reduced by 25% compared to RABBIT (see Section III-C). In these experiments, it is worth noting that, although the training and testing sets come from different sources, the proposed method is still capable of yielding good performance.

D. Speed

Less computation cost requirement is one of the key advantages of the proposed method. Upon the LONI LPBA40 data set (with a size of 220 × 220 × 184) used in the previous section, we compared the average computation cost of our proposed method incorporating HAMMER, diffeomorphic demons, FNIRT, ART, and SyN with that of the original counterpart. In Fig. 10, we show the execution time for both before and after integration with our method. In addition, achieving better registration accuracy as described in Section III-B, our method takes only 4, 1.05, 13, 3, and 11 min after integrating HAMMER, diffeomorphic demons, FNIRT, ART, and SyN, respectively, with our framework. Without our framework, the original five methods need 42, 3.2, 40, 9, and 31 min, respectively. This implies a reduction in the computation time by 10-fold, 3-fold, 3-fold, 3-fold, and 2.8-fold for these five methods, respectively. It is worth noting that we used the same set of parameters for the same registration algorithm, with its binary codes downloaded from the respective website. For the prediction of the initial deformation in our method, it only takes 5 s on average. Therefore, the time cost of prediction is almost negligible, as compared to 5 min by RABBIT [36]. RABBIT also reported the computation time by integrating with HAMMER on the same data set, which completes the whole process in 9 min. Compared with nearly 4 min by our method [see Fig. 10(a)], the computation time is further reduced.

IV. Conclusion

A fast deformable brain registration framework using a novel deformation prediction model has been presented. Specifically, regression models are trained to capture the correlations between brain appearances and their deformation coefficients. The learned correlation models are then used to rapidly predict a good initial deformation for any given image under registration. The IT is generated by warping the original template with the estimated initial deformation field. Since the shape difference between the IT and the given image becomes small, many existing registration methods (i.e., HAMMER, diffeomorphic demons, FNIRT, ART, or SyN), when incorporated into our framework, can perform much faster with comparable or slightly better registration performance. It is worth noting that our method can be applied to a wider range of images since it employs a parameter-free statistical model on both images and deformations.

Acknowledgments

This work was supported in part by the National Institutes of Health under Grant EB006733, Grant EB008374, and Grant EB009634, the National Basic Research Program of China (973 Program) under Grant 2010CB832505, and NSFC Grant 61075010. The associate editor coordinating the review of this manuscript and approving it for publication was Prof. Sina Farsiu.

References

1. Job DE, Whalley HC, McConnell S, Glabus M, Johnstone EC, Lawrie SM. Voxel-based morphometry of gray matter densities in subjects at high risk of schizophrenia. Schizophr. Res. 2003 Nov.vol. 64(no. 1):1–13. [PubMed: 14511796]
2. Frisoni G, Testa C, Zorzan A, Sabattoli F, Beltramello A, Soininen H, Laakso M. Detection of gray matter loss in mild Alzheimer's disease with voxel based morphometry. J. Neurol. Neurosurg. Psychiatry. 2002 Dec.vol. 73(no. 6):657–664. [PubMed: 12438466]
3. Merschhemke M, Mitchell TN, Free SL, Hammers A, Kinton L, Siddiqui A, Stevens J, Kendall B, Meencke HJ, Duncan JS. Quantitative MRI detects abnormalities in relatives of patients with epilepsy and malformations of cortical development. NeuroImage. 2003 Mar.vol. 18(no. 3):642–649. [PubMed: 12667841]
4. Thompson PM, Mega MS, Woods RP, Zoumalan CI, Lindshield CJ, Blanton RE, Moussai J, Holmes CJ, Cummings JL, Toga AW. Cortical change in Alzheimer's disease detected with a disease-specific population-based brain atlas. Cerebral Cortex. 2001 Jan.vol. 11(no. 1):1–16. [PubMed: 11113031]
5. Freeborough PA, Fox NC. Modeling brain deformations in Alzheimer's disease by fluid registration of serial 3-D MR images. J. Comput. Assist. Tomogr. 1998 Sep-Oct;vol. 22(no. 5):838–843. [PubMed: 9754126]
6. Downhill JE, Buchsbaum MS, Wei T, Spiegel-Cohen J, Hazlett EA, Haznedar MM, Silverman J, Siever LJ. Shape and size of the corpus callosum in schizophrenia and schizotypal personality disorder. Schizophr. Res. 2000 May; vol. 42(no. 3):193–208. [PubMed: 10785578]
7. Rueckert D, Sonoda LI, Hayes C, Hill DLG, Leach MO, Hawkes DJ. Non-rigid registration using free-form deformations: Application to breast MR images. IEEE Trans. Med. Imag. 1999 Aug.vol. 18(no. 8):712–721.
8. Johnson HJ, Christensen GE. Consistent landmark and intensity-based image registration. IEEE Trans. Med. Imag. 2002 May; vol. 21(no. 5):450–461.
9. Thirion JP. Image matching as a diffusion process: An analogy with Maxwell's demons. Med. Image Anal. 1998 Sep.vol. 2(no. 3):243–260. [PubMed: 9873902]
10. Rohr K. Image registration based on thin plate splines and local estimates of anisotropic landmark localization uncertainties. Proc. MICCAI. 1999:1174–1183.
11. Shen D, Davatzikos C. HAMMER: Hierarchical attribute matching mechanism for elastic registration. IEEE Trans. Med. Imag. 2002 Nov.vol. 21(no. 11):1421–1439.

12. Shen D, Davatzikos C. Very high resolution morphometry using mass-preserving deformations and HAMMER elastic registration. NeuroImage. 2003 Jan.vol. 18(no. 1):28–41. [PubMed: 12507441]
13. Shen, D. Proc. MICCAI. France: St. Malo; 2004. Image registration by hierarchical matching of local spatial intensity histograms; p. 582-590.
14. Ou Y, Sotiras A, Paragios N, Davatzikos C. DRAMMS: Deformable registration via attribute matching and mutual-saliency weighting. Med. Image Anal. 2011 Aug.vol. 15(no. 4):622–639. [PubMed: 20688559]
15. Bajcsy R, Kovacic S. Multiresolution elastic matching. Comput. Vis. Graph. Image Process. 1989 Apr.vol. 46(no. 1):1–21.
16. Davatzikos C. Spatial transformation and registration of brain images using elastically deformable models. Comput. Vis. Image Understand. 1997 May; vol. 66(no. 2):207–222.
17. Christensen G, Rabbitt RD, Miller MI. Deformable templates using large deformation kinematics. IEEE Trans. Image Process. 1996 Oct.vol. 5(no. 10):1435–1447. [PubMed: 18290061]
18. Christensen G, Rabbitt RD, Miller MI. 3D brain mapping using a deformable neuroanatomy. Phys. Med. Biol. 1994 Mar.vol. 39(no. 3):609–618. [PubMed: 15551602]
19. Ferrant, M.; Warfield, S.; Nabavi, A.; Macq, B.; Kikinis, R. Registration of 3-D intraoperative MR images of the brain using a finite element biomechanical model; Proc. 3rd Int. Conf. Med. Image Comput. Comput.-Assisted Intervention; Pittsburgh, PA. 2000.
20. Glocker B, Komodakis K, Navab N, Tziritas G, Paragions N. Dense registration with deformation priors. Proc. IPMI. 2009; vol. 5636:540–551. LNCS.
21. Loeckx D, Makes F, Vandermeulen D, Suetens P. Non-rigid image registration using a statistical spline deformation model. Proc. IPMI. 2003; vol. 2732:463–474. LNCS.
22. Xue Z, Shen D, Davatzikos C. Statistical representation of high-dimensional deformation fields with application to statistically-constrained 3-D warping. Med. Image Anal. 2006 Oct.vol. 10(no. 5):740–751. [PubMed: 16887376]
23. Rueckert D, Frangi AF, Schnabel JA. Automatic construction of 3-D statistical deformation models of the brain using nonrigid registration. IEEE Trans. Med. Imag. 2003 Aug.vol. 22(no. 8): 1014–1025.
24. Albrecht, T.; Luthi, M.; Vetter, T. A statistical deformation prior for non-rigid image and shape registration; Proc. IEEE Conf. CVPR; 2008. p. 1-8.
25. Vercauteren T, Pennec X, Perchant A, Ayache N. Diffeomorphic demons: Efficient non-parametric image registration. NeuroImage. 2009 Mar.vol. 45(no. 1):S61–S72. [PubMed: 19041946]
26. Andersson, J.; Smith, S.; Jenkinson, M. FNIRT—FMRIB's nonlinear image registration tool; Proc. 14th Annu. Meeting Org. HBM; 2008.
27. Ardekani BA, Guckemus S, Bachman A, Hoptman MJ, Wojtaszek M, Nierenberg J. Quantitative comparison of algorithms for inter-subject registration of 3-D volumetric brain MRI scans. J. Neurosci. Methods. 2005 Mar.vol. 142(no. 1):67–76. [PubMed: 15652618]
28. Avants BB, Epstein CL, Grossman M, Gee JC. Symmetric diffeomorphic image registration with cross-correlation: Evaluating automated labeling of elderly and neurodegenerative brain. Med. Image Anal. 2008 Feb.vol. 12(no. 1):26–41. [PubMed: 17659998]
29. Klein A, Andersson J, Ardekani BA, Ashburner J, Avants B, Chiang MC, Christensen GE, Collins DL, Gee J, Hellier P, Song JH, Jenkinson M, Lepage C, Rueckert D, Thompson P, Vercauteren T, Woods RP, Mann JJ, Parsey RV. Evaluation of 14 nonlinear deformation algorithms applied to human brain MRI registration. NeuroImage. 2009 Jul.vol. 46(no. 3):786–802. [PubMed: 19195496]
30. Minh Hoai N, Fernando T. Metric learning for image alignment. Int. J. Comput. Vis. 2010 May; vol. 88(no. 1):69–84.
31. Jiang, J.; Zheng, S.; Toga, AW.; Tu, Z. Learning based coarse-to-fine image registration; Proc. IEEE Conf. CVPR; 2008. p. 1-7.
32. Lee, D.; Hofmann, M.; Steinke, F.; Altun, Y.; Cahill, ND.; Schölkopf, B. Learning similarity measure for multi-modal 3-D image registration; Proc. IEEE Conf. Comput. Vis. Pattern Recog; 2009. p. 186-193.
33. Wu G, Qi F, Shen D. Learning-based deformable registration of MR brain images. IEEE Trans. Med. Imag. 2006 Sep.vol. 25(no. 9):1145–1157.

34. Wu, G.; Qi, F.; Shen, D. Proc. IPMI. The Netherlands: Kerkrade; 2007. Learning best features and deformation statistics for hierarchical registration of MR brain images; p. 160-171.
35. Yeo BTT, Sabuncu MR, Vercauteren T, Holt DJ, Amunts K, Zilles K, Golland P, Fischl B. Learning task-optimal registration cost functions for localizing cytoarchitecture and function in the cerebral cortex. IEEE Trans. Med. Imag. 2010 Jul.vol. 29(no. 7):1424–1441.
36. Tang S, Fan Y, Wu G, Kim M, Shen D. RABBIT: Rapid alignment of brains by building intermediate templates. NeuroImage. 2009 Oct.vol. 47(no. 4):1277–1287. [PubMed: 19285145]
37. Tian, Y.; Narasimhan, SG. A globally optimal data-driven approach for image distortion estimation; Proc. IEEE Conf. CVPR; 2010. p. 1277-1284.
38. Christensen GE, Johnson HJ. Consistent image registration. IEEE Trans. Med. Imag. 2001 Jul.vol. 20(no. 7):568–582.
39. Cootes TF, Edwards GJ, Taylor CJ. Active appearance models. IEEE Trans. Pattern Anal. Mach. Intell. 2001 Jun.vol. 23(no. 6):681–685.
40. Collobert T, Bengio S. SVMTorch: Support vector machine for large-scale regression problems. J. Mach. Learn. Res. 2001; vol. 1:143–160.
41. Smola AJ, Scholköpf B. A tutorial on support vector regression. Statist. Comput. 2004 Aug.vol. 14(no. 3):199–222.
42. Burges CJC. A tutorial on support vector machines for pattern recognition. Data Mining Knowl. Discov. 1998 Jun.vol. 2(no. 2):121–167.
43. Cherkassky V, Ma Y. Selection of meta-parameters for support vector regression. Proc. ICANN. 2002; vol. 2415:687–693. LNCS.
44. Smith SM, Jenkinson M, Woolrich MW, Beckmann CF, Behrens TEJ, Johansen-Berg H, Bannister PR, Luca MD, Drobnjak I, Flitney DE, Niazy R, Saunders J, Vickers J, Zhang Y, Stefano ND, Brady JM, Matthews PM. Advances in functional and structural MR image analysis and implementation as FSL. NeuroImage. 2004; vol. 23:208–219.
45. Christenson GE, Geng X, Kuhl JG, Bruss J, Grabowski TJ, Pirwanu IA, Vannier MW, Allen JS, Damasio H. Introduction to the Non-rigid image registration evaluation project (NIREP). Proc. 3rd Int. Workshop Biomed. Image Registration. 2006; vol. 4057:128–135. LNCS.
46. Shattuck DW, Mirza M, Adisetiyo V, Hojatkashani C, Salamon G, Narr KL, Poldrack RA, Bilder RM, Toga AW. Construction of a 3-D probabilistic atlas of human cortical structures. NeuroImage. 2008 Feb.vol. 39(no. 3):1064–1080. [PubMed: 18037310]
47. Xue Z, Shen D, Karacali B, Stern J, Rottenberg D, Davatzikos C. Simulating deformations of MR brain images for validation of atlas-based segmentation and registration algorithms. NeuroImage. 2006 Nov.vol. 33(no. 3):855–866. [PubMed: 16997578]
48. Resnick SM, Goldszal A, Davatzikos C, Golski S, Kraut MA, Metter EJ, Bryan RN, Zonderman AB. One-year age changes in MRI brain volumes in older adults. Cerebral Cortex. 2000 May; vol. 10(no. 5):464–472. [PubMed: 10847596]
49. Van Rijsbergen, CJ. Information Retrieval. London, U.K.: Butterworth-Heinemann; 1979.
50. Marcus DS, Wang TH, Parker J, Csernansky JG, Morris JC, Buckerner RL. Open Access Series of Imaging Studies (OASIS): Cross-sectional MRI data in young, middle aged, nondemented, and demented older adults. J. Cogn. Neurosci. 2007 Sep.vol. 19(no. 9):1498–1507. [PubMed: 17714011]

Biographies

Minjeong Kim received the Ph.D. degree in computer science and engineering from Ewha Womans University, Seoul, Korea.

She is currently with the Image Display, Enhancement, and Analysis Research Laboratory, The University of North Carolina, Chapel Hill, as a Postdoctoral Research Associate. Her research interests cover image registration, segmentation, and machine learning approaches in medical image analysis.

She has served as a reviewer for international journals and conferences in medical image analysis.

Guorong Wu received the Ph.D. degree in computer science and engineering from Shanghai Jiao Tong University, Shanghai, China.

He is currently with the Image Display, Enhancement, and Analysis Research Laboratory, The University of North Carolina, Chapel Hill, as a Postdoctoral Research Associate. His research interests are image registration and machine learning in medical image analysis.

Pew-Thian Yap received the Ph.D. degree in image processing from the University of Malaya, Kuala Lumpur, Malaysia, in 2007.

He is an Assistant Professor of radiology with the Department of Radiology and the Biomedical Research Imaging Center, The University of North Carolina, Chapel Hill. He has made vital technical contributions to human brain mapping by developing novel algorithms for diffusion-weighted magnetic resonance imaging (DW-MRI) data, ranging from the popular diffusion tensor imaging to the high- precision high angular resolution diffusion imaging. His major research interest is in DW-MRI and its application to the characterization of brain white-matter connectivity. His current research focuses on the clinical application of these technical innovations and the development of next-generation cutting-edge neuroimaging technologies. In particular, he has employed a tract-based approach to characterize brain white-matter connectivity of pediatric subjects, giving fundamentally important neuropsychological insights into human brain development in the first years of life. His current efforts are being directed at extending this framework to incorporate information from different imaging modalities (structural MRI + functional MRI + DW-MRI) and applying this novel analysis paradigm to a number of important clinical studies, including Alzheimer’s disease, schizophrenia, and multiple sclerosis, for both prognosis and diagnosis purposes.

Dinggang Shen was a Tenure-Track Assistant Professor with the University of Pennsylvania and a Faculty Member with the Johns Hopkins University. He is currently a Professor of radiology, computer science, and biomedical engineering with the Department of Radiology and the Biomedical Research Imaging Center (BRIC), The University of North Carolina, Chapel Hill. He is also the Director of the Image Display, Enhancement, and Analysis Laboratory in the Department of Radiology and of the medical image analysis core in the BRIC. He has published more than 300 papers in international journals and conference proceedings. His research interests include medical image analysis, computer vision, and pattern recognition.

Prof. Shen serves as an Editorial Board Member for four international journals.

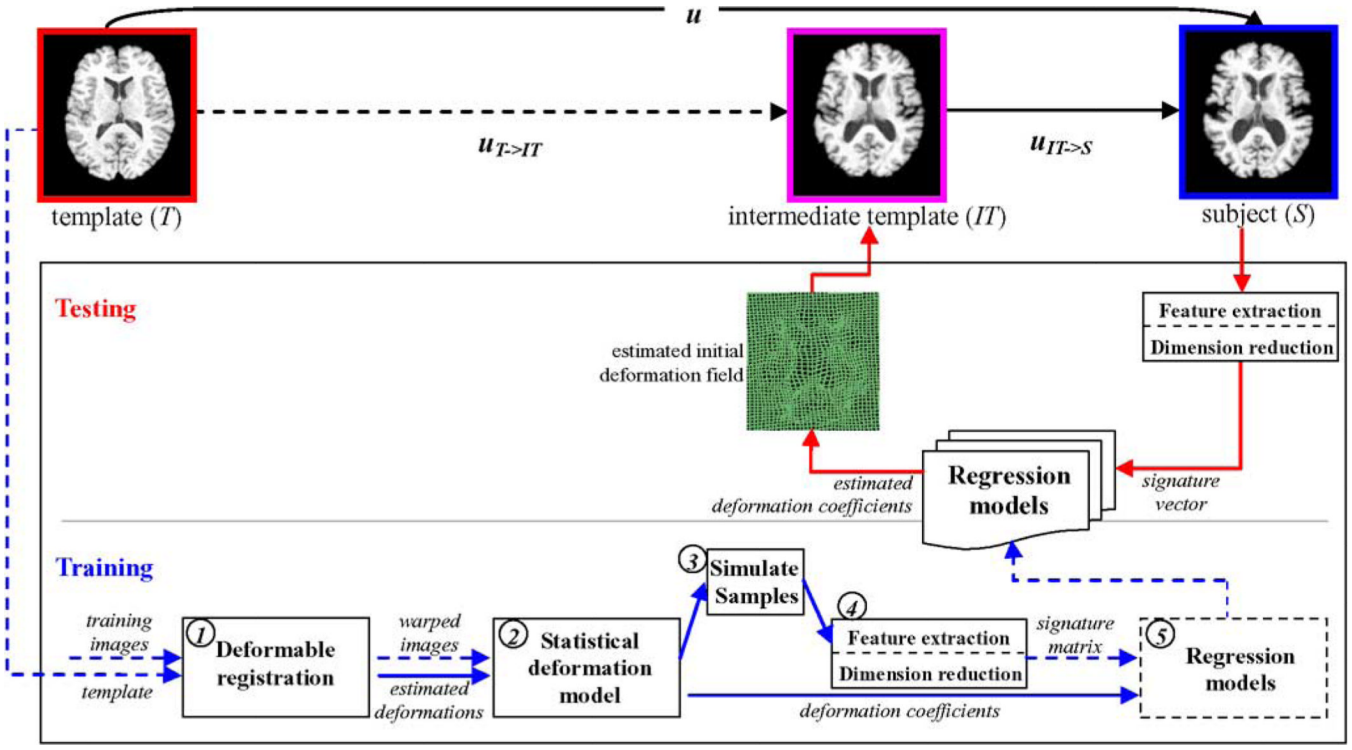

Fig. 1.

Overview of the proposed learning-based registration framework. Initial deformation field $u_{T\rightarrow IT}$ and the IT are predicted by the SVR models trained with deformation coefficients and brain appearances (based on the training and testing stages, as shown in the large black rectangle). Blue arrows represent the processes in the training stage, whereas red arrows represent the processes in the testing stage. A registration algorithm is needed only to estimate the residual deformation from the IT (in the pink rectangle) to the subject (in the blue rectangle). (See Section II-A for more information.)

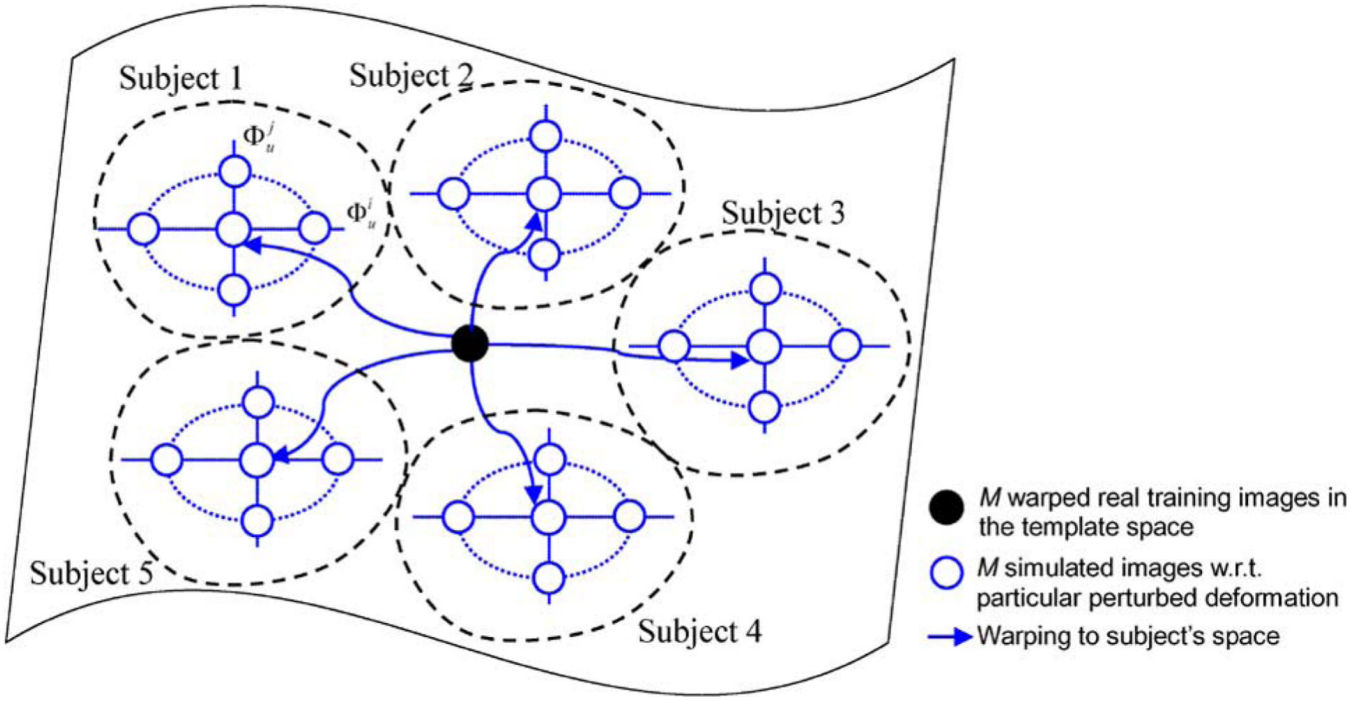

Fig. 2.

Illustration of how new sample images are simulated in the training stage. In this example, there are five subjects ($M = 5$), each with four perturbations ($N = 4$). Each large dotted black circle denotes a set of M images generated for each subject j, $j = 0, 1, \ldots, N$.

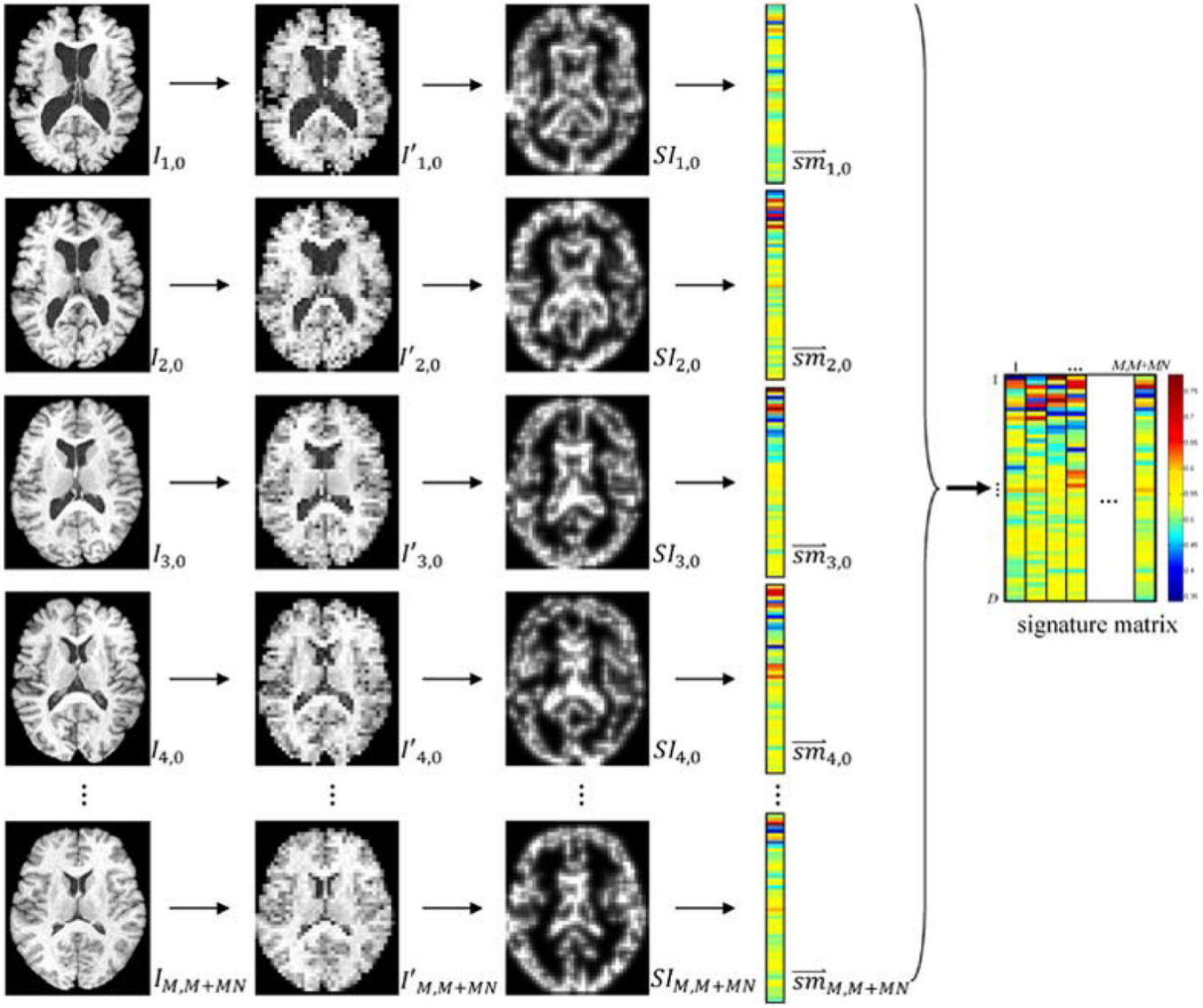

Fig. 3.

Brain appearance model. The brain images after removal of uninformative background voxels are shown in the leftmost column, with their downsampled versions given in the second column. PCA is then applied to the signature images, as shown in the third column, which consist of the brain outlines and the boundaries along the interfaces of WM, GM, CSF, and VN. The fourth column denotes the signature vectors (projections onto the D eigenvectors) for $\{\tilde{I}_{i,k}\}$ after reconstruction with only the top D eigenvectors, and they can be agglomerated into a matrix SM, as displayed in the rightmost column.

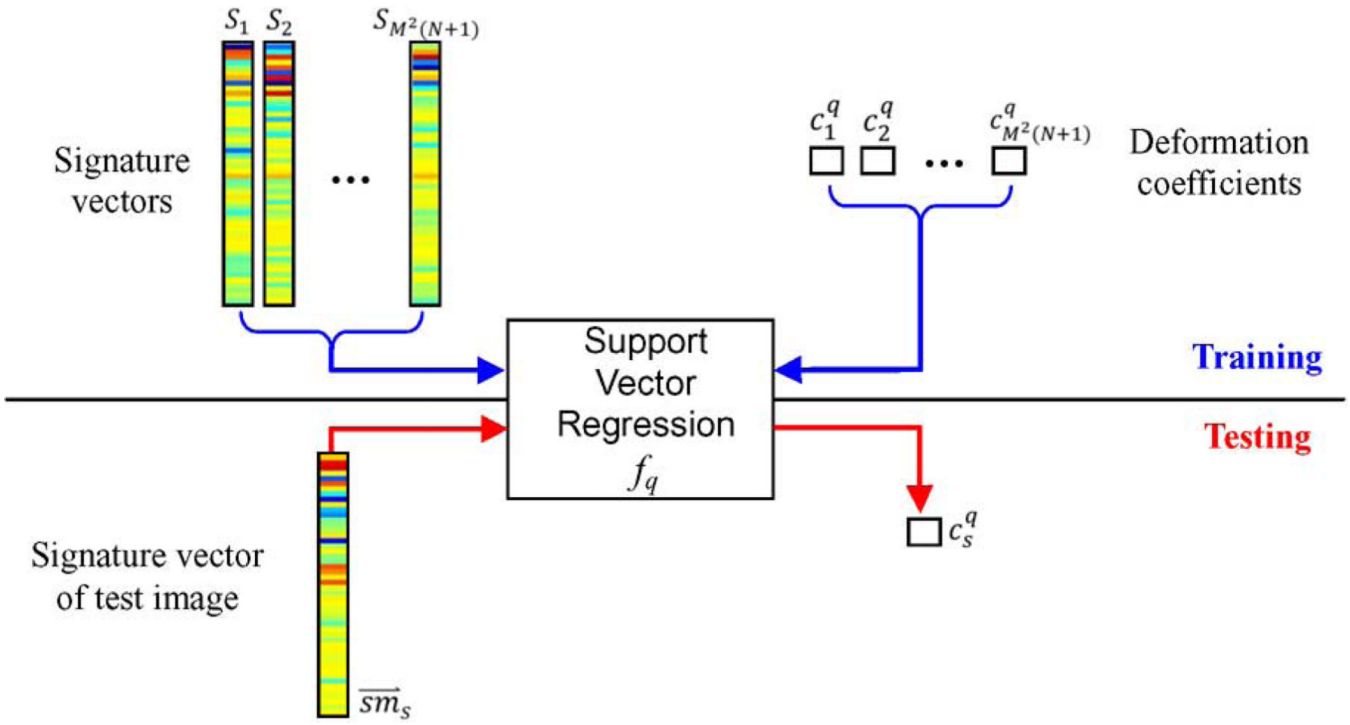

Fig. 4.

*q*th SVR among *Q* models used to correlate signature vectors with the *q*th row of deformation coefficient matrix *C*. (Blue arrows) Features (signature vectors) and target values (the *q*th row of the deformation coefficient matrix) used for training the *q*th regression model. (Red arrows) Prediction of deformation coefficients for a new subject image. By feeding the signature vector of the subject image to the learned SVR models, the deformation coefficient c_s^q for the subject image can be predicted.

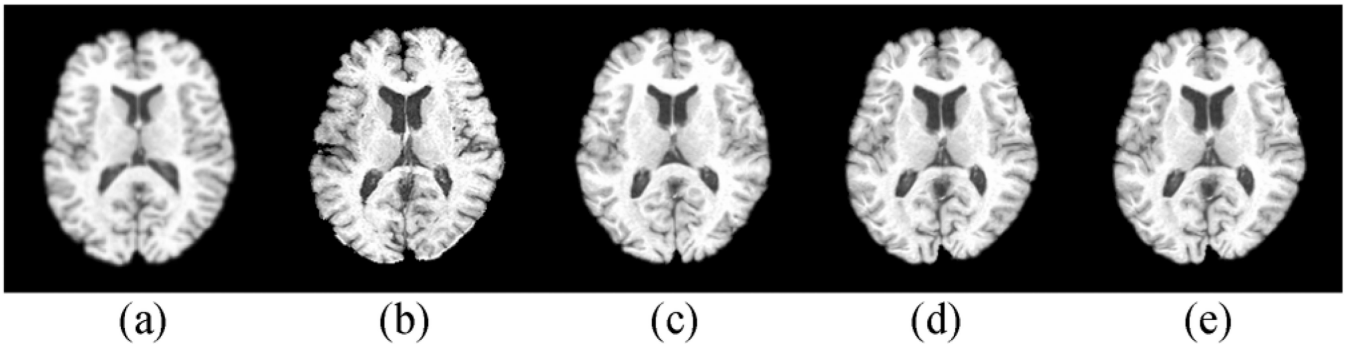

Fig. 5.
Illustration of the proposed registration algorithm in aligning (b) a subject image with (a) a template image. (c) An IT is estimated, onto which (b) the subject image can be registered. By concatenating the deformation fields from the template to the IT and from the IT to the subject, we can warp the template to the subject, as shown in (d), which is comparable to the results given by HAMMER, as shown in (e).

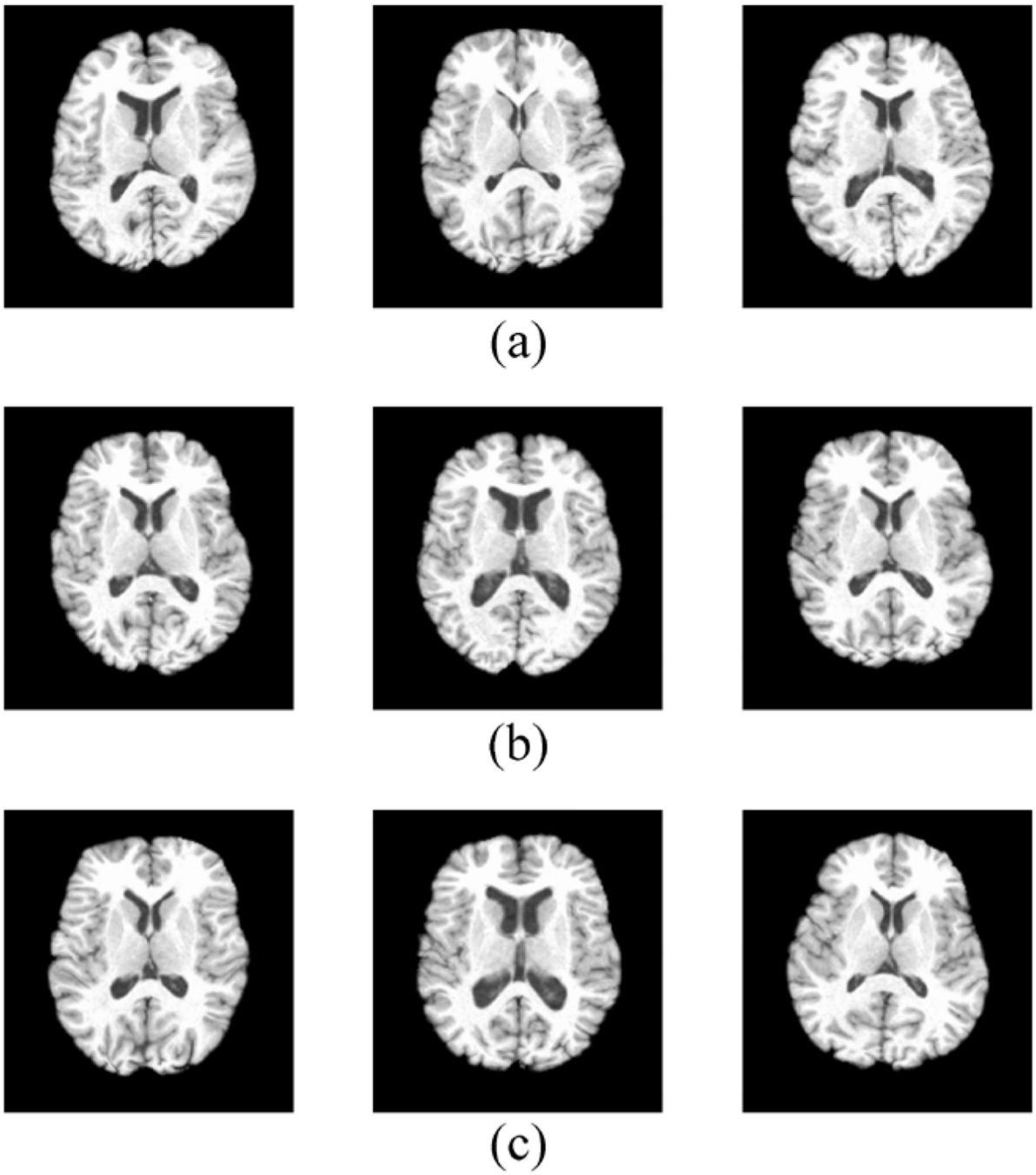

Fig. 6.
Simulated images generated by warping the template with the simulated deformation fields. According to the extent of deformation from the template, the simulated images are classified into three groups: 2 mm (Group 1), 4 mm (Group 2), and 6 mm (Group 3). (a) Group 1. (b) Group 2. (c) Group 3.

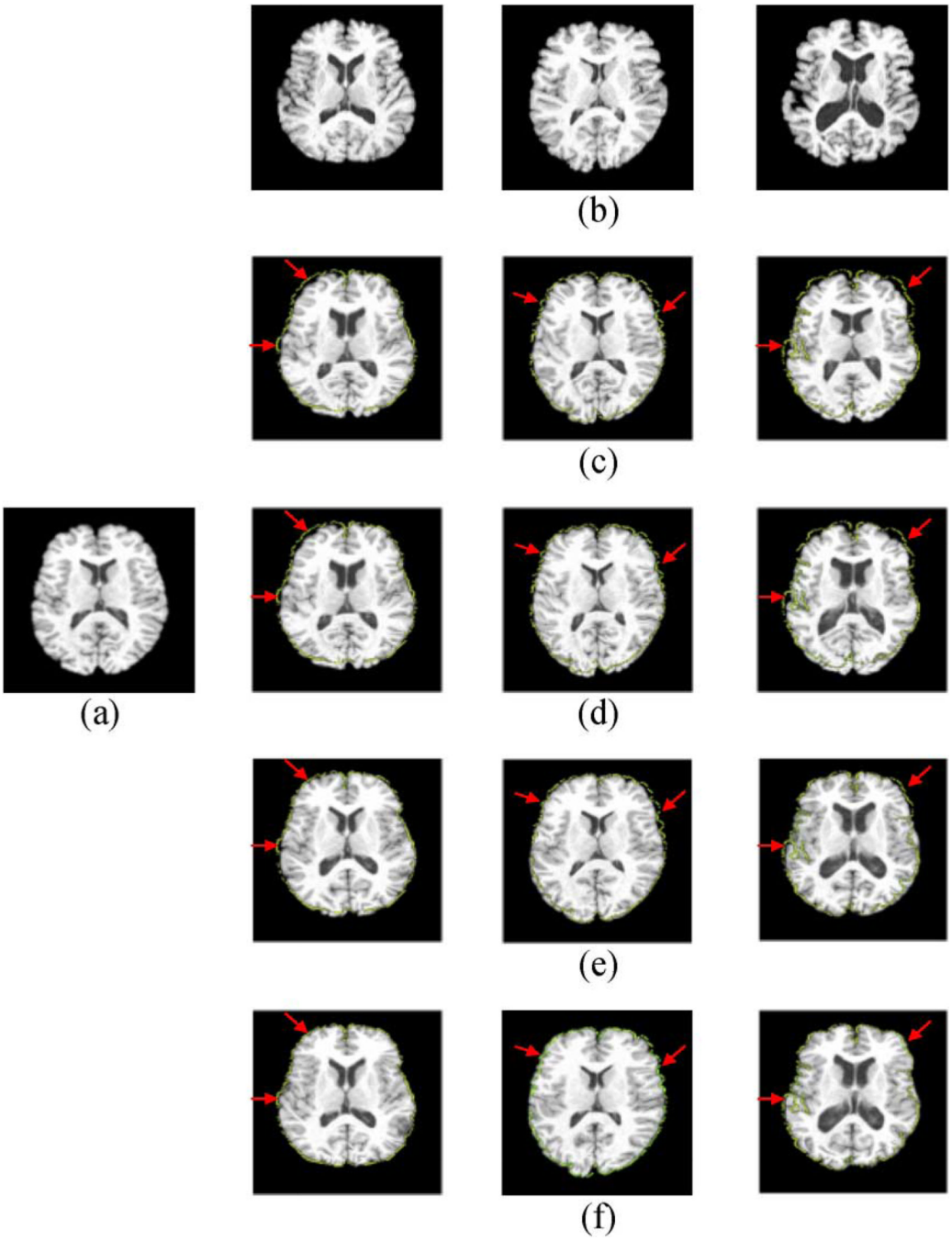

Fig. 7.

Estimation of (f) the ITs for (b) the subject images by the proposed method. The estimated ITs have a closer resemblance to the subject images than (a) the original template. Compared with the results of HAMMER in (c) low resolution, (d) middle resolution, and (e) RABBIT, our results show better performance (indicated by the red arrows). For visual comparison, we overlay the brain outlines of the subject images onto the respective ITs or intermediate registration results by HAMMER.

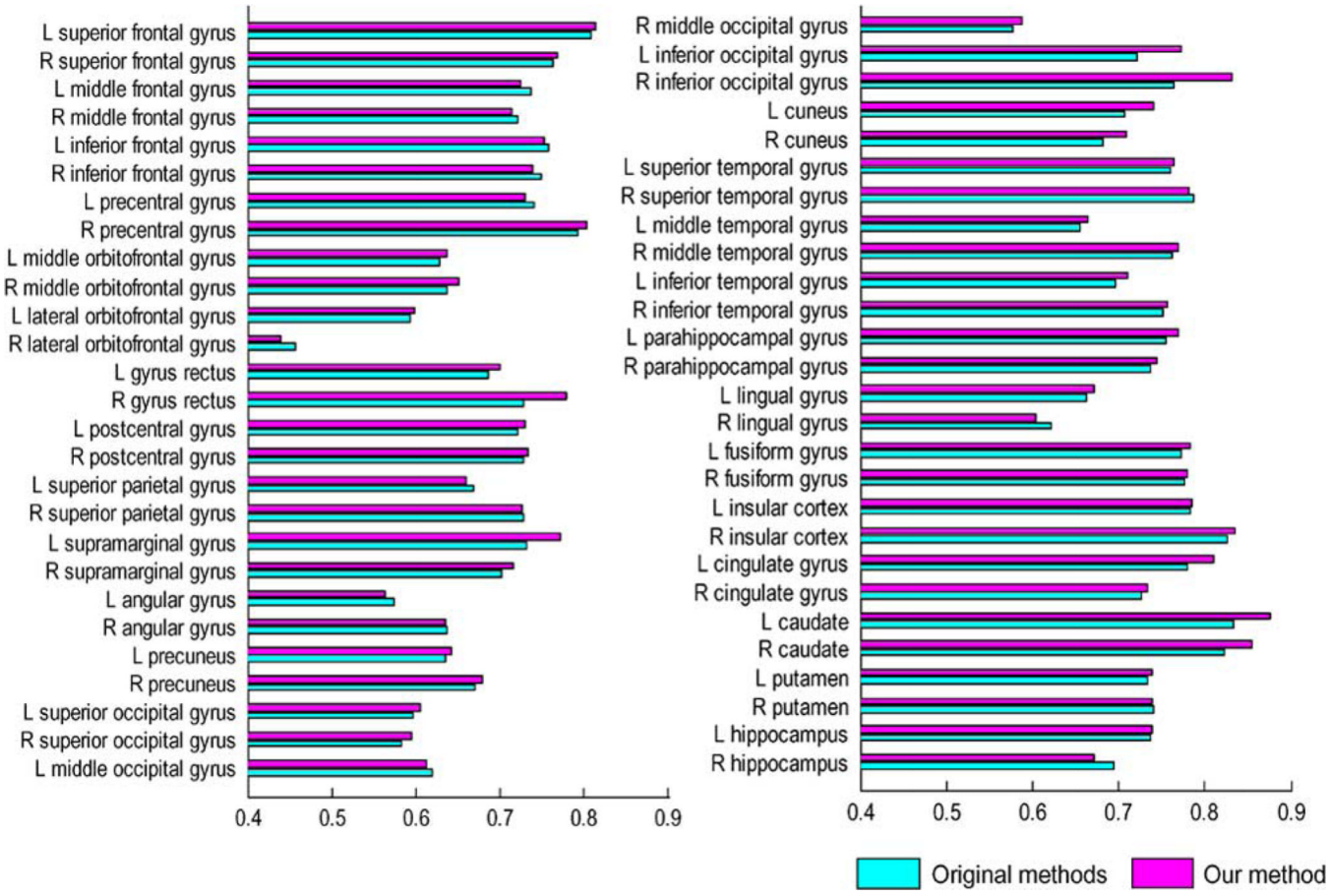

Fig. 8.

Mean overlap ratios of 54 manually delineated ROIs given by five registration methods (i.e., HAMMER, diffeomorphic demons, FNIRT, ART, and SyN) on average with and without our framework. The LONI LPBA40 data set was used.

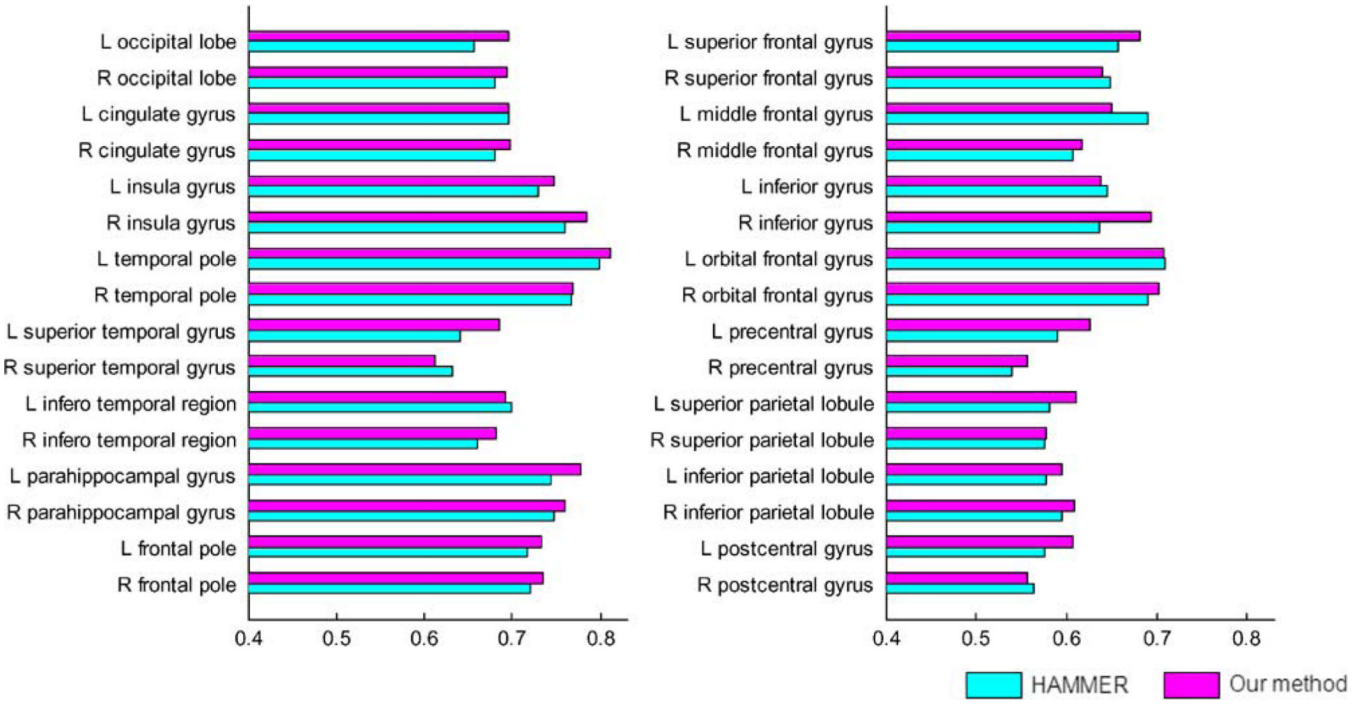

Fig. 9.
Mean overlap ratios on 32 manually delineated ROIs of the NIREP data set.

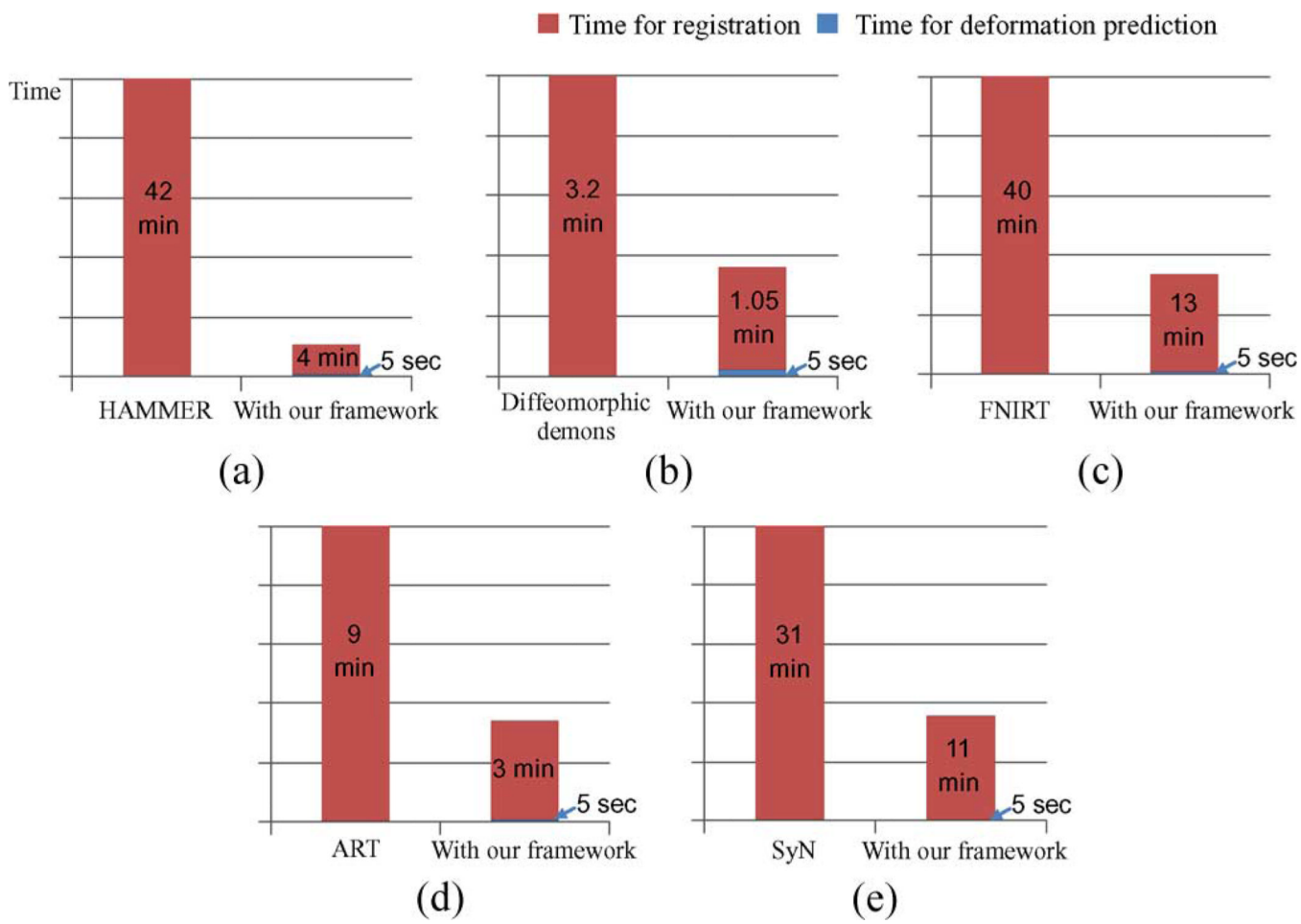

Fig. 10.

Comparison of computation times for HAMMER, diffeomorphic demons, FNIRT, ART, and SyN before and after integration with our learning-based deformation prediction framework. (a) HAMMER. (b) Diffeomorphic demons. (c) FNIRT. (d) ART. (e) SyN.

TABLE I

Mean Registration Error Evaluated With Respect to the Ground Truth (in Millimeters)

	Group1	Group2	Group3	Average
HAMMER	0.44	0.49	0.62	0.52
RABBIT	0.36	0.47	0.53	0.45
Our Method	0.35	0.37	0.46	0.39

TABLE II

Average Overlap Ratios (in Percent) of WM, GM, and VN, Computed Based on 50 Testing Subjects

	WM	GM	VN	Overall
HAMMER (low re.)	60.3%	50.4%	49.4%	53.4%
HAMMER (mid res.)	64.1%	58.3%	64.9%	62.4%
RABBIT	71.8%	64.7%	77.3%	71.3%
Our Method	77.4%	70.3%	85.6%	77.8%

TABLE III

Average Dice Ratios Before and After Integration of HAMMER, Diffeomorphic Demons, FNIRT, ART, and SyN With Our Framework. The Improvement For All Cases Is Statistically Significant ($p < 0.05$, Two-Sample t-Test)

	HAMMER	Diff. Demons	FNIRT	ART	SyN
Before	71.1%	70.1%	69.9%	70.3%	72.6%
After	72.0%	72.0%	70.5%	71.0%	73.3%